frontiers | Frontiers in Marine Science

TYPE Original Research
PUBLISHED 02 September 2024
DOI 10.3389/fmars.2024.1427579

OPEN ACCESS

EDITED BY
Selvaraj Kandasamy,
Central University of Tamil Nadu, India

REVIEWED BY
Madhavaraju Jayagopal,
National Autonomous University of Mexico, Mexico
Anmol Barla,
Central University of Tamil Nadu, India
Xing Jian,
Xiamen University, China

*CORRESPONDENCE
Ce Wang
wangce@mail.sysu.edu.cn

RECEIVED 04 May 2024
ACCEPTED 30 July 2024
PUBLISHED 02 September 2024

CITATION
Cui H, Wang C, Su M, Lei Y, Zeng L and Jia J (2024) Detrital zircons record the provenance and source-to-sink process in the northwestern margin of the South China Sea. *Front. Mar. Sci.* 11:1427579. doi: 10.3389/fmars.2024.1427579

Detrital zircons record the provenance and source-to-sink process in the northwestern margin of the South China Sea

Heqi Cui[1,2], Ce Wang[1,2,3]*, Ming Su[1,2,3], Yaping Lei[1,2], Letian Zeng[1,2] and Junmin Jia[1,2]

[1]School of Marine Sciences, Sun Yat-sen University, Zhuhai, China, [2]Guangdong Provincial Key Laboratory of Marine Resources and Coastal Engineering, Zhuhai, China, [3]Southern Marine Science and Engineering Guangdong Laboratory (Zhuhai), Zhuhai, China

The northwestern continental margin of the South China Sea, extending from the broad shelf and canyon-growth slope across the Xisha Trough, represents a relic crustal rift that eventually connects to the abyssal plain. However, the provenance and source-to-sink process of sediments in this special topography remains unclear. In this study, we present the detrital zircon U-Pb geochronology of surface sediments from the northwestern margin of the South China Sea to identify the sediment provenance, track the transport pathway, and understand the source-to-sink process in this margin. The results showed that detrital zircons exhibit a wide range of U-Pb ages from 3,062.9 to 41.5 Ma and are characterized by peaks centered on 140–154 Ma, 240–258 Ma, 425–452 Ma, and 738–991 Ma. Statistical analysis indicated that the clastic sediments on the shelf closely resemble those sourced from the Pearl River system. Conversely, sediments on the slope and abyssal plain demonstrated characteristics indicative of multiple sources, primarily originating from the Pearl River, with a minor contribution from the Red River. Further quantitative study revealed a progressive increase (from 8.2% to 43.2%) in the prevalence of Red River-derived sediments with ascending water depth on the shelf and slope, whereas sediment influx in the deepest sector remains predominantly sourced from the Pearl River. This study emphasizes the controls of topography and currents in modulating the transportation of coarse-grained and fine-grained sediments within the source-to-sink system and provides a favorable solution for reconstructing the sedimentary process in continental margins.

KEYWORDS

provenance, detrital zircon, U-Pb geochronology, source-to-sink, continental margin, South China Sea

1 Introduction

The connection between mountain and abyssal regions is established through the source-to-sink process, which shapes modern landscapes and leaves lasting geological history. This process is influenced heterogeneously by lithology, tectonics, climate, and ocean currents (Bentley et al., 2016; Caracciolo, 2020). The continental margin, receiving sediments from various sources, undergoes control and molding by the source-to-sink process. Acting as a bridge between terrestrial and deep-sea environments, the continental margin holds enormous terrigenous detritus, which helps in understanding sedimentation patterns and the underlying evolutionary mechanisms (Hu et al., 2012; Milliman and Farnsworth, 2013; Clift et al., 2014; Romans et al., 2016).

The northwestern continental margin of the South China Sea (SCS) encompasses diverse topographies, providing a natural laboratory for studying provenance and sedimentary processes. A notable area is the northwestern continental margin of the SCS, where the Xisha Trough is situated (Figure 1B). This region includes four distinct topographic units that form a board zone of shallow to deep water: the continental shelf and slope, Xisha Trough, and Northwest Sub-basin of the SCS (Figure 1B). Understanding the provenance of these sediments is crucial for regional tectonics,

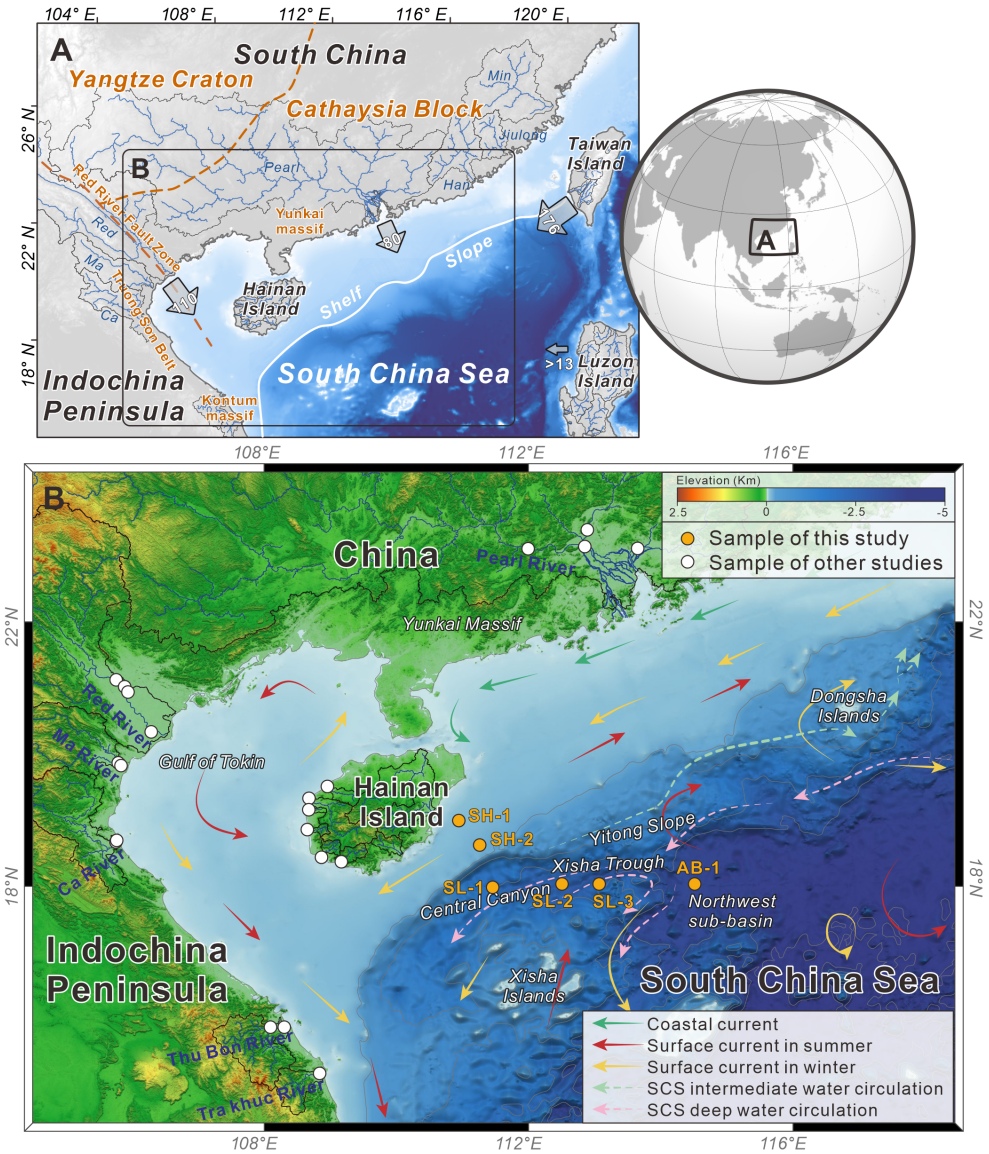

FIGURE 1
(A) Tectonic map and the major source drainage systems of the northwestern South China Sea. The tectonic boundaries of the blocks are compiled from van Hoang et al. (2009) and He et al. (2020). The arrows indicate the annual suspended sediments (Mt/yr) for major drainage systems, as depicted in Milliman and Farnsworth (2013). **(B)** Topographic map of the northwestern South China Sea showing the drainage systems and sample locations in this study. Compiled detrital zircon studies follow Cao et al. (2023). The locations near estuaries are chosen to represent riverine discharge. Potential sources include the Pearl River (Zhao et al., 2015a; Liu et al., 2017), Red River (Clift et al., 2006; Fyhn et al., 2019; Wang et al., 2019), coastal rivers in central Vietnam (Fyhn et al., 2019; Wang et al., 2019), and coastal rivers in Hainan (Wang et al., 2015). The major currents of the northwestern SCS are depicted by arrow lines and are collected from Liu et al. (2016) and Chen et al. (2021).

ocean currents, and natural resource exploration (Wang et al., 2014; Sharman et al., 2015; Liu et al., 2016). Previous studies investigated the surface sediments through bulk geochemistry, Sr-Nd isotopes, and grain size, and suggested that the primary sources of fine-grained detritus to the Xisha Trough were the Pearl River and Taiwan (Zhong et al., 2017b; Liu et al., 2018; Cai et al., 2020). Seismic and zircon geochronology provenance analyses focused on the time period from the Oligocene to the Quaternary revealed that the sediment supply through the Central Canyon system was gravity-driven (Su et al., 2015; Zhao et al., 2015b; Li et al., 2017), whereas shelf sediments predominantly originated from the Pearl River and are influenced by coastal and surface currents (Zhong et al., 2017a). Studies on clay minerals indicated that fine-grained sediment is mainly derived from Taiwan Island (approximately 50–70%), as well as from the Red River and Vietnam (Liu et al., 2014a, 2016; Cai et al., 2020).

Despite extensive research, the transportation of sediments in the northwestern SCS remains unclear. Coarse-grained sediments, such as silt and sand, are often overlooked, even though they can constitute up to 50% of the abyssal plain's sediments (Liu et al., 2014a; Zhong et al., 2017b). Previous studies have focused on the bulk or fine-grained sediments, neglecting coarse fractions necessary for comprehensive provenance analysis. Limited data from the deep-water area further hinder understanding of the source-to-sink process in this sedimentary system (Liu et al., 2014a, 2016, 2018; Cai et al., 2020). Accurately determining sediment provenance requires the identification of transport pathways and the evaluation of contributions from multiple sources.

U-Pb dating of detrital zircon is a powerful tool for provenance analysis (Gehrels, 2011; Cao et al., 2023). Zircon, a common and durable mineral, preserves information about the magmatic events of source rocks (Gehrels, 2011). By matching detrital zircon ages with potential sources, the provenance of sediments can be determined (Wang et al., 2019). The application of detrital zircon U-Pb geochronology, along with statistical measures, articulates further detail in provenance studies (Gehrels, 2011; Vermeesch, 2013; Dodson et al., 2022). Recent advancements in the detrital zircon geochronology method have brought about more quantitative approaches for elucidating the provenance of sediments, offering a more precise method of deciphering the sediment process in the margin (Sharman and Johnstone, 2017; Sundell and Saylor, 2017; Cao et al., 2018).

From shelf to abyssal plain, the East Asian margin's large river deltas and sedimentary systems are influenced by tectonics, monsoons, sea level changes, ocean currents, and human activities (Li et al., 2014; Gao and Collins, 2014), which also control the river channel migration and delta evolution of the Mississippi margin (Bentley et al., 2016) and Bengal Fan (Blum et al., 2018). This study aims to clarify the relationship between surface sediments and the surrounding fluvial catchments by interpreting the compilation of detrital zircon U-Pb geochronology. It seeks to uncover the provenance of coarse-grained sediments and combine that of published fine-grained sediments to provide a comprehensive view of sedimentation patterns in the northwestern margin of the SCS. Further quantitatively assessing the contribution of sources will offer insights into sediment transport pathways and the influence of topography and currents within the source-to-sink system.

2 Geological setting

The SCS is one of the largest marginal seas in the western Pacific Ocean, with its northern boundary marked by South China, the Indochina Peninsula, and the islands of Hainan, Luzon, and Taiwan (Figure 1A). These terranes annually deliver approximately 416 Mt of clastic detritus to the suspended sediments of the northern SCS through the inland fluvial catchments (Milliman and Farnsworth, 2013). The seafloor of the SCS spread between 33 and 15 Ma but ceased after the Eurasia plate started subducting under the Philippine Sea plate, which caused the contemporaneous uplift of Taiwan island (Taylor and Hayes, 1983). The propagation of the SCS seafloor induced the spreading of the Northwest Sub-basin along the northside of the Zhongsha-Xisha massif approximately after 33 Ma, subsequently forming the Xisha Trough as a failed rift arm (Sun et al., 2006, 2009; Lei and Ren, 2016). The tectonic rift of the Xisha Trough proceeded during the Oligocene and consequently generated thinned continental crust from approximately 25 to 8 km overlaying the Cenozoic sediments.

The study area spans from the continental shelf along the eastern margin of the Hainan Islands into the abyssal plain toward the southeast, extending eastward into the SCS, traversing a depth of 100 to 3,500 m (Figure 1B). The continental shelf has a smooth and broad appearance and is generally shallower than 200 m, extending southeastwardly approximately 100–300 km to the continental shelf break. The continental slope growth submarine canyons, these gullies connect to the east-west trending Xisha Trough (Figure 1B). The seafloor within the trough axis exhibits an eastward tilt, with depths gradually increasing from 1,500 to 3,400 m, and the easternmost edge connects with the abyssal plain (Figure 1B). The Northwest Sub-basin is flat and situated on the abyssal plain with a depth exceeding 3,000 m, with mafic seamounts scattered internally.

The ocean currents within the SCS basin typically divide into three distinct water masses based on their depth, encompassing surface currents, intermediate water circulation, and deep-water currents (Wang et al., 2016; Zhu et al., 2019). The surface current is primarily forced by seasonal monsoon wind stress and simultaneously influenced by the Kuroshio intrusion (Su, 2004; Xue et al., 2004). In the winter, a southwestward wind covers the atmosphere of the SCS, generating a cyclonic basin-scale current in the surface layer of the SCS (Qu, 2000; Liu et al., 2001). Conversely, in summer, a northeastward wind induces an anticyclonic surface current, forming the annual dynamic pattern of the surface layer (Qu, 2000; Liu et al., 2001). Intermediate water circulation is generally anticyclonic along the continental slope in the north, driven by the inflow of North Pacific Intermediate Water through the Luzon Strait, mostly at depths approximately 1,000 m (Zhu et al., 2010; Wang et al., 2013a). A series of mesoscale eddies distribute on the northern slope driven by the Kuroshio current and internal wave. The Northern Pacific Deep Water invades the SCS

through the Luzon strait, then sinks and flows westward, forcing a basin-scale deep cyclonic gyre that eventually develops as deep-water currents (Qu et al., 2006; Wang et al., 2011).

3 Characteristics of potential sources

Understanding the spatial variation of age modes is required to recognize the characters of source terranes. Therefore, potential source characters should be established firstly by compiling detrital zircon U-Pb geochronology data of the potential sources. Previous studies illustrated that the sediments in the northwestern SCS are mainly derived from four potential source terranes: the Pearl River, Red River, Hainan Island, and central Vietnam (Lei et al., 2020). The source regions are influenced by widespread events, including the Caledonian (400–540 Ma), Hercynian-Indosinian (220–270 Ma), and Yanshanian (80–180 Ma) orogenies. The Caledonian event in the South China Block is generally considered an intracontinental collision during the early Paleozoic era (Wang et al., 2007b). The Indosinian orogeny, initially defined in the Indochina Block in Vietnam, was later recognized as a Triassic thermotectonic event affecting the South China Block (Lepvrier et al., 2004; Wang et al., 2013b). Widespread Triassic igneous activity, metamorphism, and deformation have been revealed by several studies (Li et al., 2006; Wang et al., 2013b). The Yanshanian orogeny (80-180 Ma), characterized by extensive continental margin magmatism and metamorphism, is associated with plate movements and block collisions (Zhou and Li, 2000; Wang et al., 2013b). To effectively trace the provenance of sediments, we compiled detrital zircon ages from the major drainage systems in these source regions (Clift et al., 2006; Wang et al., 2015, 2019; Fyhn et al., 2019; He et al., 2020). These drainage systems display distinct age characteristics, indicating that they were derived from heterogeneous source regions (Figures 2B–H).

The Pearl River originates westernmost from the Yunnan-Guizhou Plateau, flows eastward across the Yangtze Craton, and then downstream flows into the Cathaysia Block (Figure 1A). The ensemble of Yangtze and Cathaysia blocks collided during the Jinning orogeny between 800 and 1,000 Ma (Wang et al., 2007a), resulting in the simultaneous formation of igneous and metamorphic rocks, which corresponds to the Neoproterozoic age population observed in this river. Yangtze Craton mainly consists of carbonates, dolostones, and siliciclastic red beds, which contribute sediments to the western catchment and are characterized by prominent peaks at approximately 265 and 800 Ma (He et al., 2020). By contrast, the sediments in the eastern catchment are derived from the Cathaysia block, where granites and minor volcanic rocks are predominantly exposed (John et al., 1990;

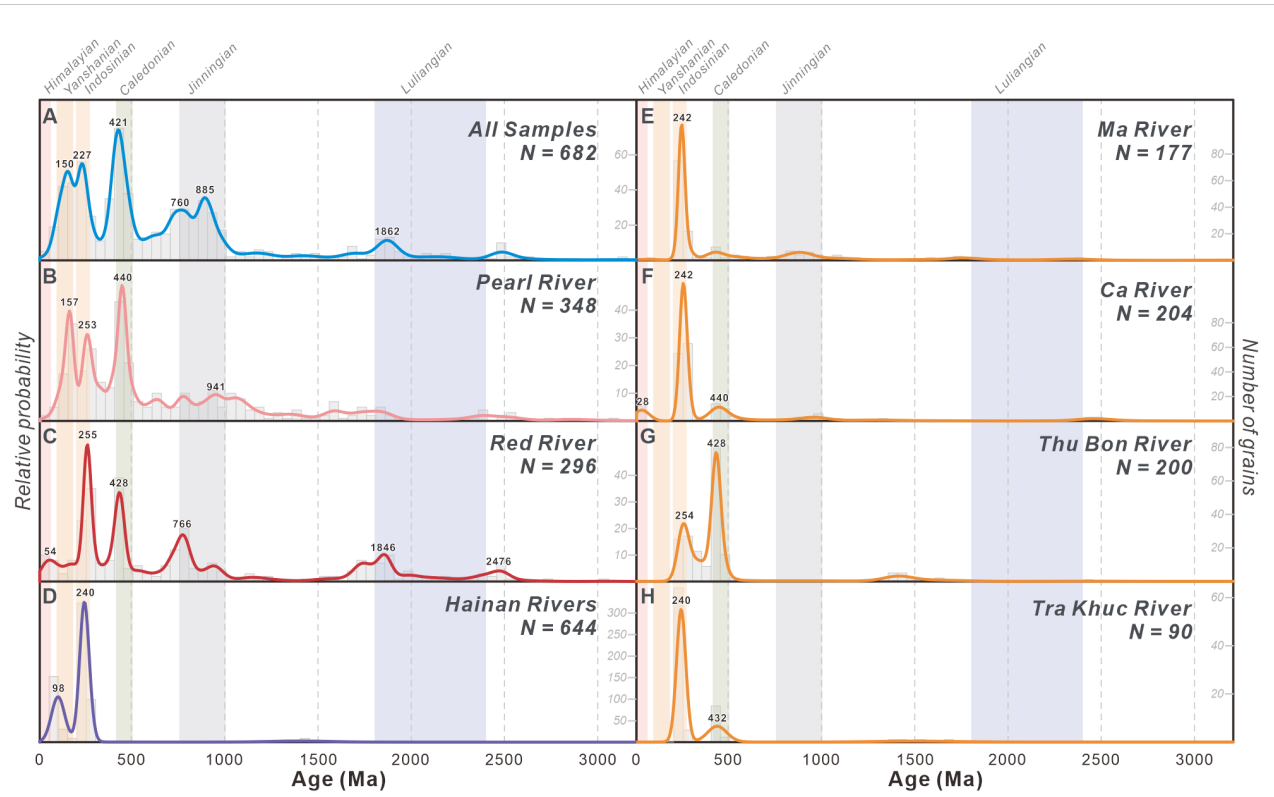

FIGURE 2
(A-H) KDE plots of potential source drainage catchments. Sample locations are shown in Figure 1B. The KDE is generated according to Vermeesch (2012) with a bandwidth of 30 Ma. The histogram, represented by gray bars, has a bin width of 50 Ma, and the count numbers are labeled on the right-hand side of each plot. The age values are marked above the peaks of the KDE curve. Colored bars show the time spans of major tectonomagmatic events. The data for the Pearl River are from Zhao et al. (2015a) and Liu et al. (2017), the data for the Red River are from Clift et al. (2006); Fyhn et al. (2019), and Wang et al. (2019), the data for the coastal rivers in central Vietnam are from Fyhn et al. (2019) and Wang et al. (2019), and the data from the coastal rivers in Hainan are from Wang et al. (2015).

Hu et al., 2013). Multimodal distribution of 160 Ma, 250 Ma, and 440 Ma corresponds to Yanshanian (80–180 Ma), Hercynian-Indosinian (220–270 Ma), and Silurian (420–440 Ma) granitic rocks, respectively, exposed in the eastern catchment (Liu et al., 2017). Age populations of approximately 2,500 Ma and 1,800–1,600 Ma are consistent with the crustal growth of the South China Block. The age population with the peak at approximately 160 Ma coincides with the extended andesitic volcanic arc province of the Eurasian plate margin (Sewell and Campbell, 2022), which produced widespread Yanshanian magmatic rocks at approximately 140 Ma in the southeast part of the Cathaysia Block, contributing a distinction mark of the Pearl River.

The Red River originates in eastern Tibet and follows along the prominent strike-slip Red River Fault Zone. It crosses the Hanoi Basin before ultimately flowing into the SCS (Figure 1A) and forming a delta in the Gulf of Tonkin. The Red River yields a wide range of zircon ages spanning from the Cenozoic to the Paleoproterozoic (Figure 2C). Indosinian granitoid intrusions and extrusive rocks expose commonly with Caledonian (400–540 Ma) intrusive rocks that occur in the Song Chay Dome and elsewhere within the southern part of the Red River catchment (Roger et al., 2000), which contribute to the 428 Ma age population in the Red River spectra. The approximate 30 Ma and 54 Ma ages derived from Eocene-Oligocene rocks of the Red River Fault Zone and the Late Cretaceous igneous rocks crop out along a fraction of the hinterland (Schärer et al., 1994; Roger et al., 2007; Xu et al., 2015). Upper reaches of the Red River erode the edge of Yangtze Craton, which experiences multiphase evolution characterized by the Jurassic (approximately 200 Ma) and Neoproterozoic (approximately 800 Ma) ages (Zhang and Schärer, 1999; Gilley et al., 2003; Clift et al., 2006; Van Hoang et al., 2009). The age populations of 1,846 Ma and 2,476 Ma are reworked via upper Red River sedimentary basins (Clift et al., 2006; Van Hoang et al., 2009). In particular, the Red River produces Neoproterozoic ages at approximately 700 Ma and exists in the Himalayan ages younger than 60 Ma. By contrast, both age populations accordingly support the distinction between the Red River-derived and Pearl River-derived sources (Figures 2B, C).

Hainan Island is situated to the south of the Leizhou Peninsula and the west of the continental shelf of the SCS (Figure 1A). The drainage systems of Hainan originate in the central hinterland, distribute radially, and flow into the SCS. The Permian to Triassic magmatism forms Yanshanian and Hercynian intrusion granites in continental arc environments, providing age signature of approximately 240 Ma in river sediments (Li et al., 2006; Xie et al., 2006). The extensional event commenced from Cretaceous formed the granites and mafic dikes during 130–90 Ma. (Wang et al., 2012; Zhou et al., 2015; Yan et al., 2017), Yanshanian granitic rocks are consequently widespread in the southern part of Hainan. These rocks contribute to the occurrence of two distinct age peaks at approximately 99 Ma and 240 Ma in the fluvial sediments (Figure 2D).

Central Vietnam comprises four major drainages that are located on the western margin of the Indochina Peninsula (Figure 1A). The northern part of the Indochina Peninsula is influenced by the Red River Fault Zone, and to the south, the Truong Son Belt borders the Kontum Massif, both of which spread Ordovician-Silurian and Permian-Triassic granitic and metamorphic rocks (Lepvrier et al., 1997; Carter et al., 2001; Shi et al., 2015). Estuary sediments of these four rivers all show dominantly age populations in Silurian and Triassic which yield resemble age modes. (Figures 2E–H). The 420–440 Ma age population exhibited in four rivers indicates the erosion of Ordovician-Silurian granites. Zircon grains derived from Permian-Triassic rocks also constitute the primary composition in the rivers. The Ca River has Cenozoic age population corresponding to Cenozoic tectonic activity that are located along the Red River Fault Zone (Figure 2F) (Wang et al., 2019). The Thu Bon River and Tra Khuc River drained from the Truong Son Belt and Kontum Massif, and display well-defined populations dominated by Permian to Triassic and Silurian age peaks (Figures 2G, H) (Roger et al., 2007; Liu et al., 2012; Wang et al., 2019).

The zircon grains in the riverine sediments are coherent with the magmatic events in catchments, and the proxies of distinguishing unequivocal regions are assured. The Pearl River is characterized by the abundant proportion of Jurassic and Early-Neoproterozoic ages, which differ from the Cenozoic and Late-Neoproterozoic ages of the Red River. The predominantly Inodosinian and Caledonian populations are insufficient to constrain Vietnam sources, but Cenozoic grains from the Red River Fault Zone can be explicitly interpreted to distinguish it from the Pearl River and Hainan sources. The Yanshanian ages with an age peak at approximately 99 Ma compose the unique age population of the Hainan and are insignificant or non-existent in other sources, delivering an efficient proxy to recognize Hainan-derived sediments.

4 Sampling and methods

Six surface sediment samples were collected from the northwestern SCS (Figure 1B). Specifically, samples SH-1 and SH-2 were obtained from the continental shelf, situated southeastern offshore of Hainan Island. Samples SL-1 and SL-2 were collect from the northern continental slope of the Central Canyon, and Sample SL-3 were from the slope of the Xisha uplift. Sample AB-1 was retrieved from the abyssal plain in the Northwest Sub-basin of the SCS. Further details about the samples are shown in Supplementary Table 1.

Zircons were extracted from samples weighing over 200 g using conventional heavy liquids and magnetic separation methods. After hand sorting under a binocular stereoscope, these zircon grains were then affixed in transparent epoxy and carefully polished to reveal their internal structures, with each grain reduced to approximately half its original size. Cathodoluminescence (CL) images were captured to discern the origins and internal structures of zircon grains, aiding in the selection of potential analysis sites (Figure 3). Zircon grains without discernible defects or overlapping zones under CL examination were picked at random for laser ablation analyses.

U-Pb dating of zircon was measured with an ELEMENT XR (Thermo Fisher Scientific) ICP-SF-MS coupled with a 193-nm (ArF)

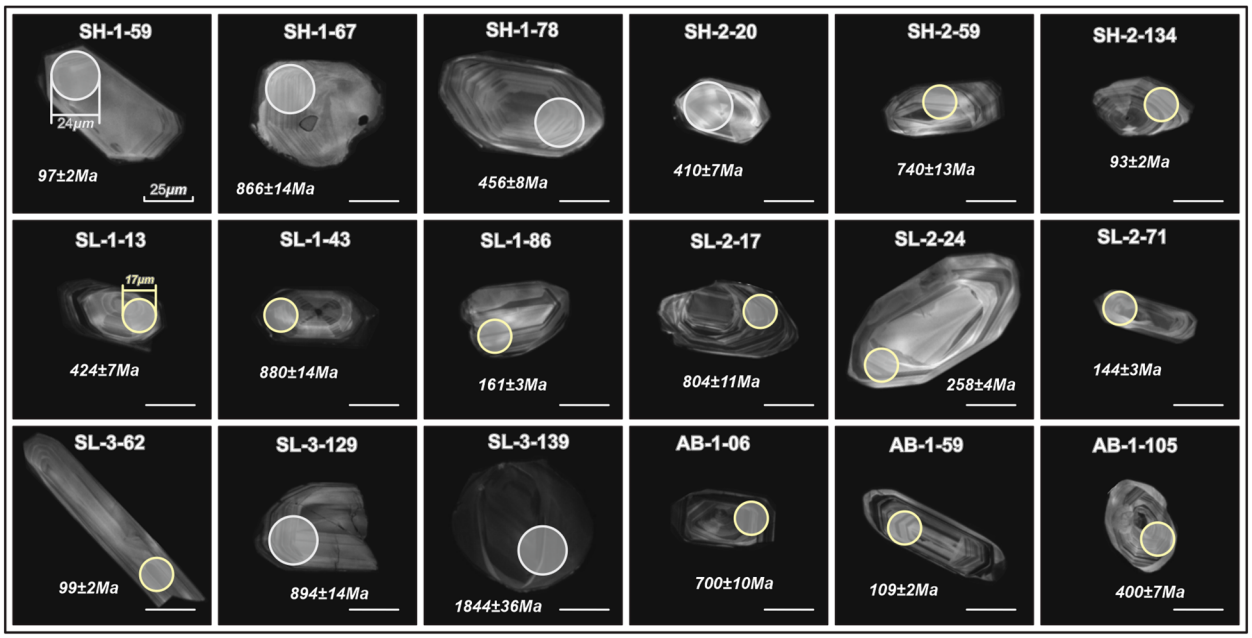

FIGURE 3
CL images of representative zircon grains for the samples from the northwestern South China Sea. White circles indicate laser ablation sites with a diameter of 24 μm, and yellow circles indicate sites with a diameter of 17 μm. The white lines represent a scale of 25 μm.

Resonetics RESOlution M-50 laser ablation system in the State Key Laboratory of Isotope Geochemistry, Guangzhou Institute of Geochemistry, Chinese Academy of Sciences. The detailed experiment procedure and data reduction strategy have been described by Zhang et al. (2018). Laser conditions were set as follows: beam sizes of 17 and 24 μm; a repetition rate of 5 Hz; and an energy density of approximately 4 J·cm^{-2}. Each spot analysis consisted of 30 s gas blank collection with the laser off, and 35 s sample signal detection with the laser on. Signals of the following masses were detected: ^{202}Hg, ^{204}(Hg+Pb), ^{206}Pb, ^{207}Pb, ^{208}Pb, ^{232}Th, and ^{238}U. The oxide molecular yield, indicated by the ^{232}Th^{16}O/^{232}Th ratio, was less than 0.3%. Zircon Plešovice (Sláma et al., 2008) and SA01 (Huang et al., 2019) were selected as the calibration standard, and every five sample analyses were followed by two analyses of Plešovice. Common Pb was corrected by ComPbCorr#3_151 using the method described by Andersen (2002).

Owing to the improving precision of ^{206}Pb/^{238}U age for younger ages and improving precision of ^{207}Pb/^{206}Pb age for older ages (Gehrels, 2011), ^{206}Pb/^{238}U ages and ^{207}Pb/^{206}Pb ages were respectively used for younger (<1 Ga) and older (>1 Ga) zircons (Gehrels et al., 2008). The concordance was defined for ages above 1 Ga using the ratio of ^{206}Pb/^{238}U and ^{207}Pb/^{206}Pb ages, and ^{207}Pb/^{235}U and ^{206}Pb/^{238}U ages were used for ages less than 1 Ga, with both calculated under 1σ level of ages. The accepted ages were selected from an 80% to 120% concordant subset. Zircon age spectrum and peaks were constructed using Kernel Density Estimation (KDE) with the R package by Vermeesch (2018). Multidimensional scaling (MDS) plots based on the Kolmogorov–Smirnov D value (KS-D value), along with the stress value indicating the fitting quality (smaller is better), were then generated to compare the detrital zircon U-Pb ages (Saylor et al., 2017). To quantitatively estimate the relative contribution of zircon grains, the Monte Carlo unmixing model based on the K-S test statistic was used in this study. The model uses the inverse Monte Carlo and forward optimization approaches of randomly reconstructing mixing samples from source samples to compare with the sink sample and determine the relative contribution ratio of the sources. The MATLAB code, detailed methods, model tests, and data applicability used have been described by Sundell and Saylor (2017).

5 Results

The zircon grains extracted from surface sediment samples were colorless to light pink and orange and had a wide range of prismatic to oval-shaped crystals. The CL images of representative zircon grains are presented in Figure 3. The predominant size range for zircon grains within the samples fell between 30 and 120 μm, which may represent a portion of the silt and sand content. The Th/U ratios of zircon grains ranged from 0.004 to 10.7, with most greater than 0.1 (Figure 4), together with oscillatory growth zoning under CL (Figure 3), pointing to a dominant igneous origin (Hoskin, 2003). In addition, 27 zircon grains yielded a Th/U value lower than 0.1 (approximately 5% of the total, Figure 4), indicating a metamorphic origin.

In total, 825 zircon grain analyses were conducted and generated 682 concordant zircon grains under uncertainties (Figure 5; Supplementary Table 2). Concordant zircon grains from this sample set showed a Mesoproterozoic to Oligocene age prevalence (1,600 to 23 Ma), representing approximately 88% of the total age population measured. Smaller populations of

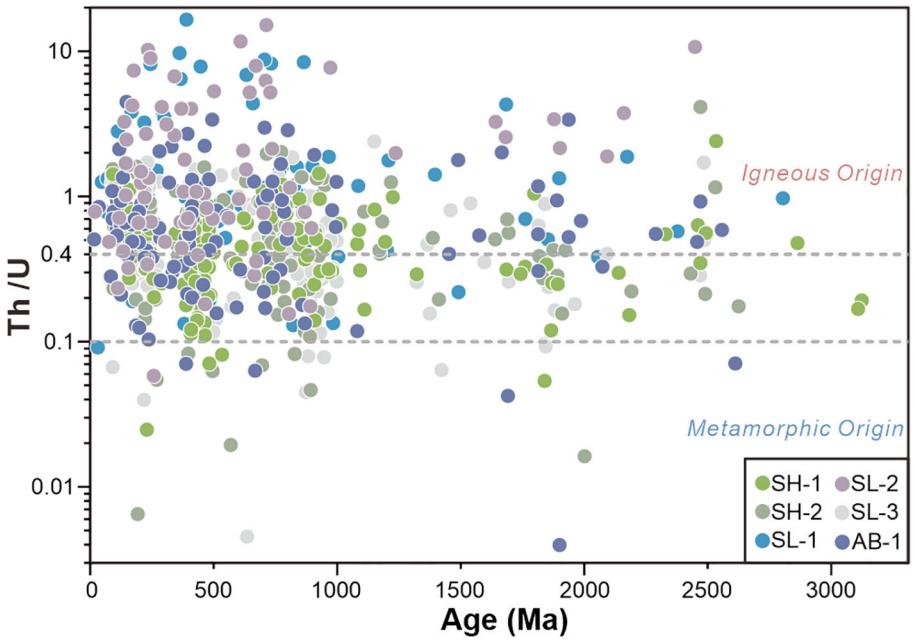

FIGURE 4
Th-U ratio plots of detrital zircons from the sediment samples in this study. A ratio greater than 0.4 indicates igneous zircons, whereas those less than 0.1 represent metamorphic zircons. A large majority (95%) of the total grains have ratios greater than 0.1, indicating a predominantly igneous origin for the zircons.

Paleoproterozoic (1,600–2,500 Ma) and Neoarchean (2,500–2,800 Ma) ages comprise between 9% to 14% of the grains in each sample (Figure 2A).

Samples SH-1 and SH-2 were collected from the continental shelf (Figure 1B). SH-1 zircons had a larger mean grain size than those of SH-2, indicating a more proximal source. Zircon crystals of both samples were characterized by oscillatory zoning. A small number of grains (approximately 10%) exhibited recrystallization domains and melt inclusion. For sample SH-1, we conducted U-Pb analyses on 153 individual zircon grains, yielding 145 concordant results within uncertainties (>80%, the same as below) (Figures 5A, B). SH-1 had a variety of ages, from the Ordovician to the Silurian, with minor Triassic to Jurassic and Neoproterozoic grains, and documented five major age peaks at approximately 158 Ma, 244 Ma, 444 Ma, 898 Ma, and 1855 Ma (Figure 6A). SH-2 included 116 concordant ages in 159 analyzed zircon grains and displayed a polymodal distribution of Jurassic, Triassic, Devonian, and Neoproterozoic ages, with six age peaks at approximately 211 Ma, 407 Ma, 735 Ma, 907 Ma, 1178 Ma, and 1890 Ma (Figure 6B). The age distributions of shelf samples differed significantly in Devonian-Ordovician ages (359-485 Ma): SH-1 showed a pronounced dominant, whereas SH-2 had a lower abundance of this age population.

Samples SL-1, SL-2, and SL-3 were collected from the continental slope (Figure 1B). CL images generally showed oscillatory zoning, several grains had the rim-core structure, and SL-2 exhibited a few long-strip shape grains. In total, 104, 94, and 157 zircon grains were analyzed, resulting in 90, 74, and 140 concordant ages for the respective samples (Figures 5C-E). These samples displayed similar polymodal age distributions with Paleogene to Cambrian and Paleoproterozoic ages, with a bimodal distribution in the Neoproterozoic (Figures 6C-E). They produced age peaks at approximately 140 Ma, 230 Ma, 420 Ma, and 700–900 Ma. Notably, each sample showed different characters in Neoproterozoic ages. Sample SL-1 generated the primary age peak at approximately 876 Ma, with a subordinary peak at approximately 763 Ma (Figure 6C). In contrast, sample SL-2 displayed the major and minor age peaks at approximately 667 Ma and 815 Ma, respectively (Figure 6D), and sample SL-3 exhibited a dominant age peak at approximately 893 Ma (Figure 6E). This observation suggests a different provenance for these sediments.

The abyssal basin sample (AB-1, Figure 1B) also showed mostly oscillatory zoning in the CL and melt inclusion was observed in several grains. The ages were determined from 117 zircon grains, which were concordant with uncertainties, out of 158 analyses performed (Figure 5F). The sample showed Jurassic, Triassic, Devonian, and Neoproterozoic age populations, and displayed five major age peaks at approximately 117 Ma, 208 Ma, 401 Ma, 482 Ma, 715 Ma, and 1915 Ma (Figure 6F). Furthermore, this sample contained three zircon grains that exhibited Archean ages.

6 Discussion

6.1 The provenance of coarse sediments

As the age signatures of the aforementioned potential sources are well-defined, the provenance of surface sediments can be identified by matching their age distribution features distinctly. The continental shelf is influenced by coastal currents and surface

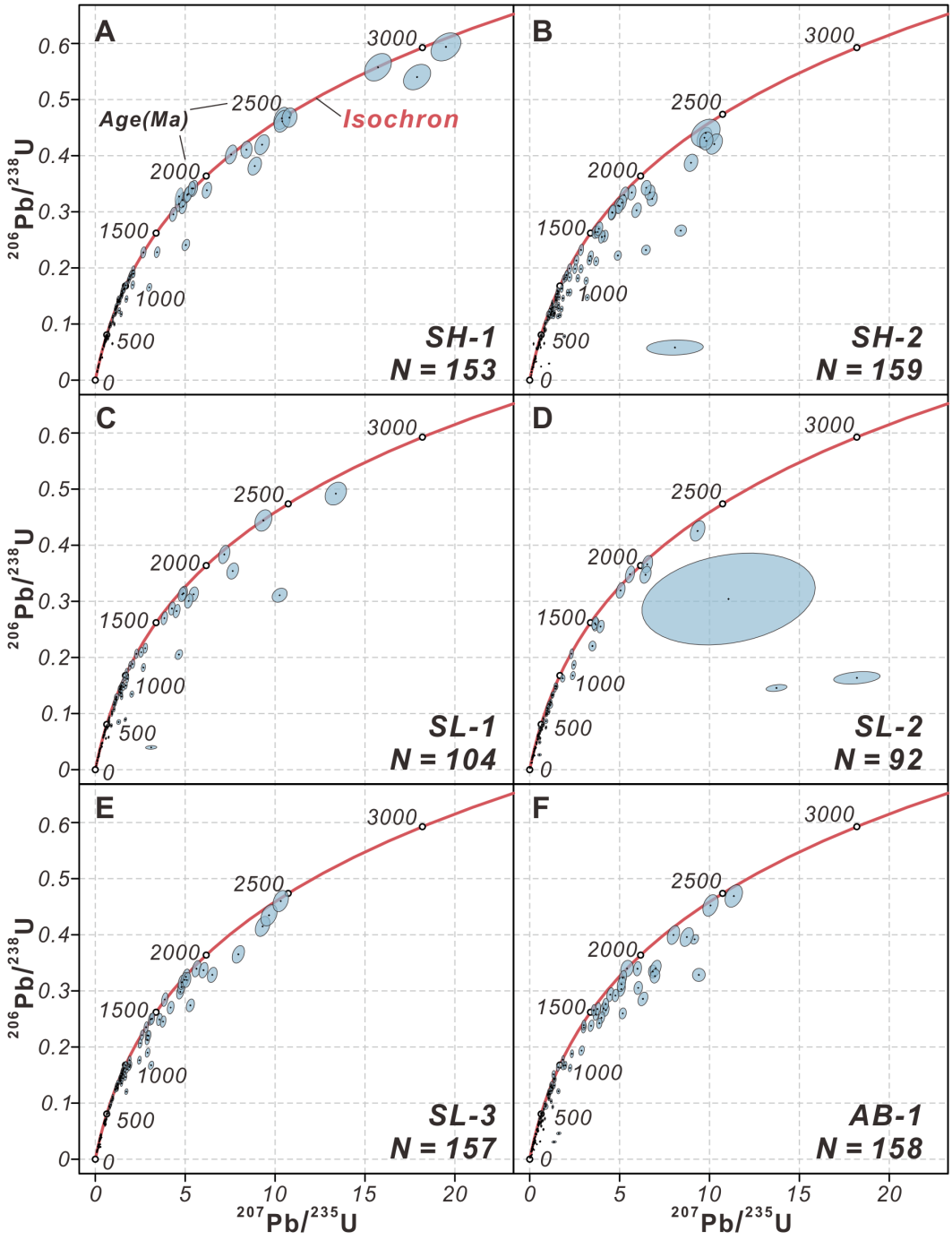

FIGURE 5
(A–F) Concordia plots of detrital zircons from the sediment samples in this study. The filled error ellipses reported all errors at 1 Sigma confidence level.

currents, transporting sediment along the southern coast of China and the southwestward downslope, respectively (Liu et al., 2014b; Zhong et al., 2017a, 2017b). Shelf sediments (samples SH-1 and SH-2) identified as the predominant Pearl River source, evidenced by the age peak of approximately 900 Ma (Figures 6A, B), reflect control of both currents. The rivers of Hainan Island and the Yunkai Massif (Figure 1A) are significant clastic contributors to the north shelf (Liu et al., 2014b; Zhong et al., 2017b; Gong et al., 2021), as indicated by the presence of the Jurassic grains and a notable Caledonian population (Figure 2D), reflecting Hainan basaltic magmatism and the Yunkai Massif (Wang et al., 2007b, 2015). Sediments from the southern continental shelf exhibit an age population of approximately 700 Ma (Figure 6B). According to age spectrum comparisons, this age population appears to be consistent with either the Red River or the Pearl River. However, sediments from the Red River are obstructed by the northern slope of the SCS, limiting their reach to the outer shelf. Moreover, sediments from the Red River typically display characteristics of Cenozoic ages

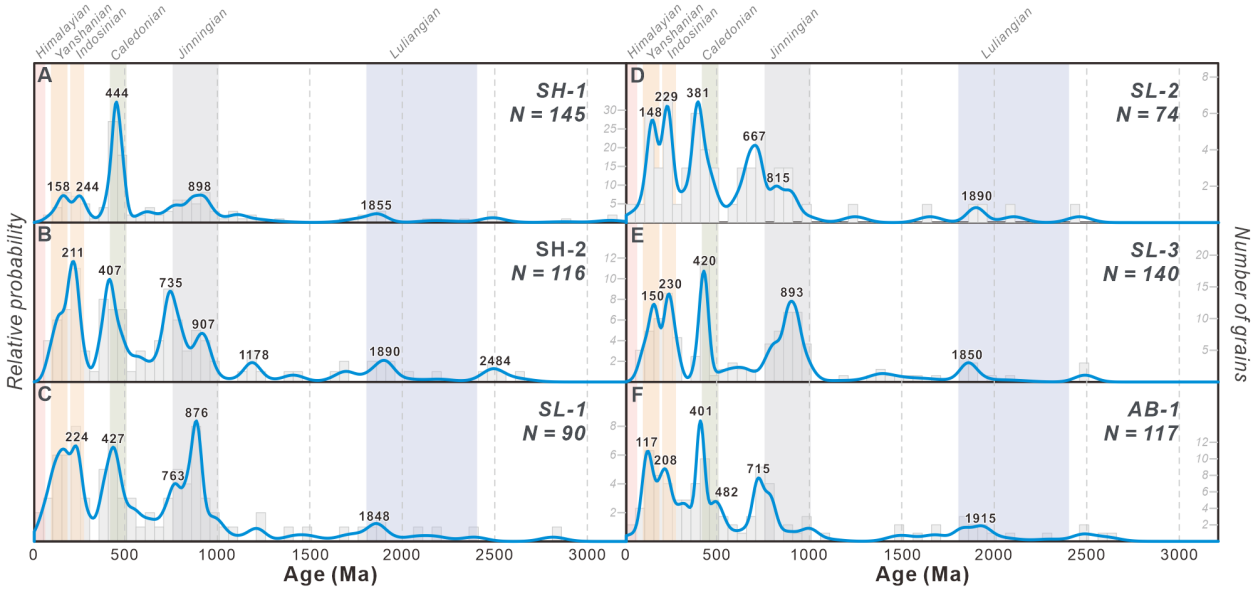

FIGURE 6
(A-F) KDE plots of detrital zircons from the sediments in the northwestern South China Sea, with the plot legend consistent with Figure 2. Sample locations are shown in Figure 1B.

(Bodet and Schärer, 2000, Clift et al., 2008, Van Hoang et al., 2009, Fyhn et al., 2019) and are notably absent in these samples. The contribution of the Red River can therefore be excluded. The western tributaries of the Pearl River drain the Yangtze Craton, producing zircons dating back to 700 Ma (Wang et al., 2007a). Hence, Pearl River sediments are suggested as the primary source on the shelf. Studies on detrital mineral and particle-reactive radionuclide assemblages (Huang et al., 2013; Hu et al., 2014) suggest that proximal Hainan-derived sediments contribute to the eastern continental shelf of Hainan Island. In the zircon ages, Jurassic grains approximately 99 Ma from shelf sediments also supported Hainan as a source. Furthermore, the cumulative distribution function (CDF) is commonly used to reveal age spectrum differences (e.g., Saylor and Sundell, 2016). In the CDF plot (Figure 7), shelf sediments closely matched that of the Pearl River but significantly differed from that of the Red River in both the 700–1,000 Ma and 1,700–1,900 Ma ranges, suggesting a dominant feed of the Pearl River source, which accords with the result of zircon ages.

The continental slope widens gradually from west to east, with its eastern bottom connecting to the Xisha Trough. Sampling locations at the bottom of the slope, the western end of the

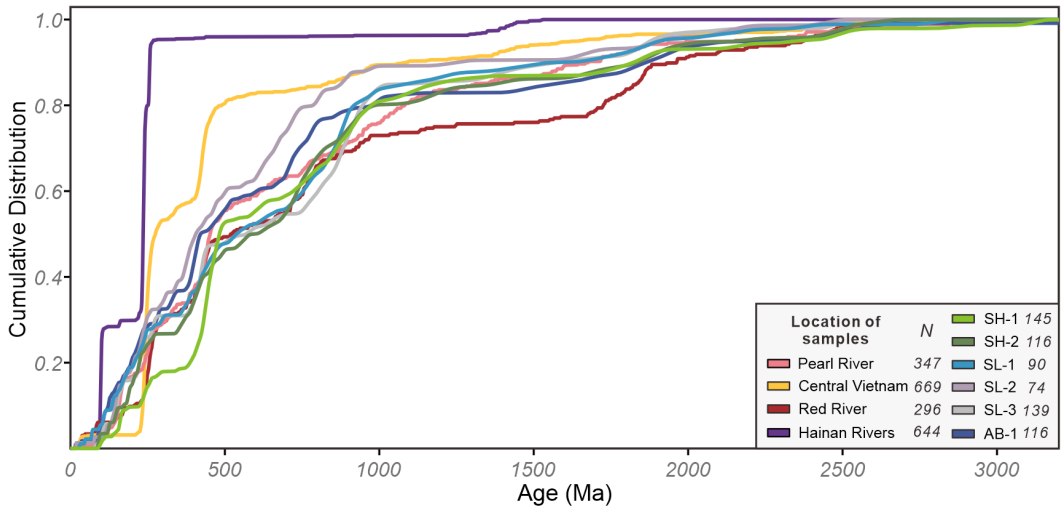

FIGURE 7
Cumulative distribution plot of detrital zircon U-Pb ages for the sediments in the northwestern South China Sea. The data are the same as in Figures 2, 6.

trough, and within the trough itself provide valuable materials for studying provenance variations along the slope (Figure 1B). The Red River has proved to be a significant source of fine-grained slope sediments. However, slope failures and slides frequently occur on the Qiongdongnan and Yitong slopes (Qin et al., 2015; Zhong and Peng, 2021). Given that detritus from the slope generally originates from the shelf (Xia et al., 2009; Zhong et al., 2017a), the provenance of turbidity deposits and the accumulation of coarse-grained fractions remains poorly defined (Liu et al., 2014a; Zhang et al., 2023). The slope sediment (samples SL-1 and SL-3) results exhibited characteristics of both the Red River and Pearl River, evidenced by abundant Cenozoic, Cretaceous-Jurassic, and Neoproterozoic grains (Figures 6C, E). Although Neoproterozoic ages with peaks at approximately 900 Ma have also been found in the rivers of southern Vietnam, southward currents hinder these sediments from reaching the north margin (Fyhn et al., 2019). Therefore, these rivers are unlikely to significantly contribute detritus to this area. In CDF curves, Yanshanian and Neoproterozoic populations in the samples align with those of the Pearl River and Red River (Figure 7), indicating a mixed-source input in this region. Hence, the provenance of sediments on the slope can be precisely attributed to a mixture of Red River and Pearl River sources. As slope failures and deep-water currents do not affect the south wall of the Xisha Trough (Chen et al., 2016; Zhang et al., 2023), the influence of the Pearl River is weaker, and Taiwan coarse sediments cannot reach this area, suggesting that the Red River may exert a greater influence in SL-3.

Sediments in the abyssal basin (AB-1) exhibited a similar age distribution to those at the western end of the trough (SL-2) (Figures 6D, F). The Xisha Trough, as a remnant rift-arm (Sun et al., 2009; Lei and Ren, 2016), shares similar tectonic and sedimentary environments with the Valencia trough, with sedimentation patterns controlled by the tilting of the faulted basement of the rift basin (Alonso et al., 1995; Su et al., 2015). These similarities create parallel longitudinal sediment transport pathways along the continental margin in two troughs. The age distribution in the abyssal basin resembles that at the western end of the trough, indicating a shared source and possibly sediment inheritance between these locations. The presence of Yanshanian ages with a peak at approximately 99 Ma provides evidence of sediment supply from Hainan in this area. Similarities between AB-1 and SL-2 are also evident in the CDF plot (Figure 7), suggesting that abyssal basin sediments originate from multiple sources, including the Pearl River, Red River, and Hainan.

MDS has emerged as a powerful analytical tool for interpreting sediment provenance in studies (Saylor et al., 2017; Wang et al., 2019; He et al., 2020). Distances between points on the MDS plot reflect dissimilarities (the KS-D value is used in this study) between samples. Closer points indicate more similar samples, whereas distant points represent greater dissimilarities (Vermeesch, 2013). This visualization in our study identified sample groups and distinguished between different source areas, providing insights into the complex mixture of sediment provenance (Figure 8). Although rivers in central Vietnam appear difficult to differentiate within samples in terms of age spectra, their dissimilarity from our samples is highlighted in the MDS plot. Even in the fine-grained sediments, central Vietnam contributes only a small amount (Liu et al., 2014a), with its characteristics hardly observed in coarse-

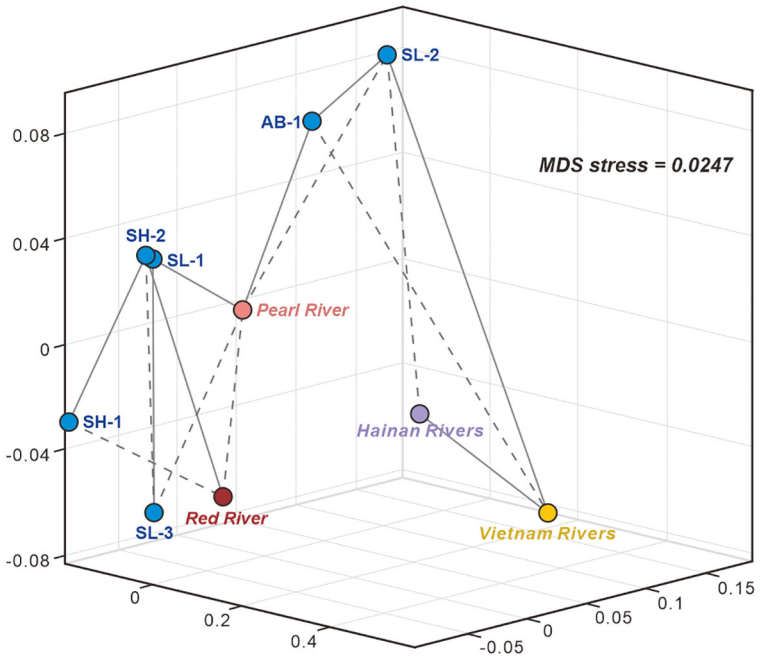

FIGURE 8
Multidimensional scaling (MDS) plot using the K-S statistic for the detrital zircon data of all potential sources and samples in this study. The data are the same as in Figures 2, 6. The solid gray lines connect the most similar samples, and the dashed gray lines connect the second most similar samples.

grained sediments. This further supports the primary deposition of sediments from this source near the eastern shelf of the Indochina Peninsula, transported southward by surface currents (Fyhn et al., 2019). Notably, our samples predominantly clustered around the Pearl River and Red River sources, clearly spatially separated from the Hainan source. The results affirm that the continental shelf sediments (samples SH-1 and SH-2) primarily originated from the Pearl River. This also validates that slope sediments (samples SL-1 and SL-3) are closest to sources from both the Pearl River and the Red River. Sample SL-2 is positioned between the Pearl River and central Vietnam in the plot, suggesting potential contributions from rivers in central Vietnam. Abyssal basin sediments (sample AB-1) plotted adjacent to SL-2 in the plot and close to the Pearl River, suggesting an inherited sediment supply and possibly a similar provenance from the Pearl River.

6.2 Coarse-grained versus fine-grained fraction

Coarse-grained and fine-grained components undergo fractionation under varying hydraulic conditions, which is common in sediment transportation (Garzanti et al., 2009; Lupker et al., 2013; Allen et al., 2015). As a high-density and large-grain mineral, the fractionation between zircon and clay minerals exists commonly (Komar, 2007; Liu et al., 2016; Garzanti et al., 2022; Jia et al., 2023). In the study area, the coarse fraction that zircon represents largely originates from the Pearl River. On the continental slope, the fine-grained fraction is primarily attributed to Taiwan and the Red River (Liu et al., 2014a; Cai et al., 2020; Zhang et al., 2023), where coarse-grained sediment (SL-1, SL-2, and SL-3) indicates a contribution from the Pearl River. The different source is likely induced by different dynamic processes. The active slide and mass transport processes occurred on the western part of the slope, providing a natural conduit for coarse sediments migrating into the slope (Qin et al., 2015; Su et al., 2015; Zhong and Peng, 2021). The coastal current and deep-water current provide a possible long-distance transport of fine-grained sediments from Taiwanese rivers to the northern SCS shelf and slope (Liu et al., 2014a; Xu et al., 2017). Notably, the low contribution (<10%) of sediment from the rivers in central Vietnam remains consistent across zircon and clay minerals (Liu et al., 2014a). This is attributed to the sediments from central Vietnam being carried southeastward, thus being unable to travel long distances to reach the study area (Fyhn et al., 2019). On the shelf (samples SH-1 and SH-2), Hainan materials are traceable in the coarse fraction but have a low content in the fine fraction (Xu et al., 2017). Hainan-derived sediments primarily settle near the coast, with coarse-grained sediments delivered by summer rainfall being particularly trapped on the continental shelf due to summer upwelling (Zhang et al., 2013; Hu et al., 2014; Xu et al., 2017).

6.3 Source contributions and sedimentary pattern

To quantitatively assess the contribution of potential sources to zircons and investigate sediment transport pathways, this study utilized the Monte Carlo method (Figure 9; Supplementary Table 3) (Sundell and Saylor, 2017). Results indicate that the continental shelf predominantly receives clastic materials derived from the Pearl River (77.9% to 91.1%), suggesting initial fluvial sediments transport to the continental shelf followed by southward movement. These sediments are transported by the coastal current and winter surface current of the northern SCS (Figure 10) (Liu et al., 2016; Zhong et al., 2017a, 2017b). Although the Red River shows a notable

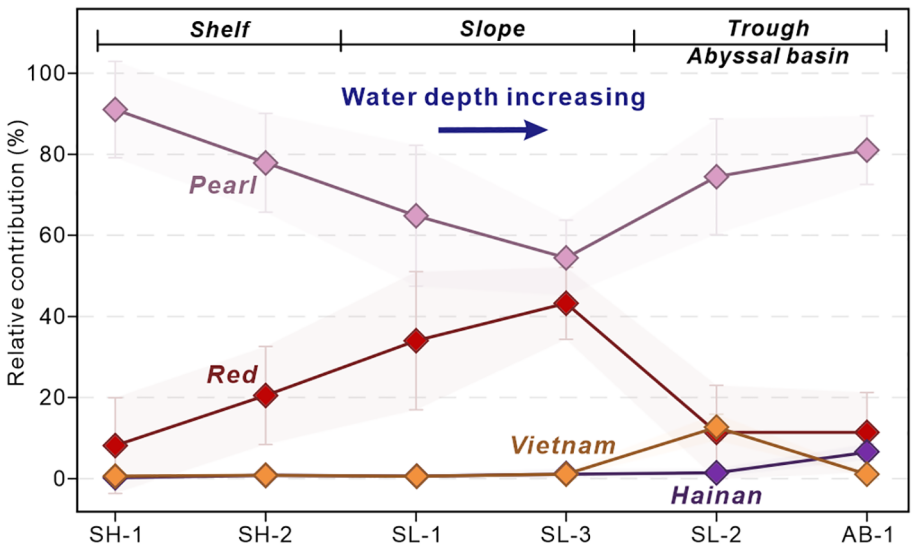

FIGURE 9
The relative contributions of potential drainage systems for the sediments in the northwestern South China Sea. The unmixing modeling was described by Sundell and Saylor (2017). The data set are the same as in Figures 2, 6.

contribution to the samples (10–20%), the absence of Cenozoic ages, as previously noted, suggests origins in the Xi River, upstream of the western Pearl River (He et al., 2020). The calculated contribution from the Red River is attributable to age population similarities between the two rivers. In this case, the Red River-derived sediments encountered obstruction by Hainan Island (Li et al., 2018) and could not reach the study area.

On the continental slope, sediments are primarily sourced from the Pearl River (54.5% to 74.6%) (Figure 9), with lesser contributions from the Red River (11.4% to 43.2%). Characterized by NW-SE- to-N-S-oriented canyons, submarine landslides, and turbidity currents (Qin et al., 2015), the continental slope provides a viable pathway for sediment transport (Figure 10). Areas with low turbidity activity primarily receive fine-grained sediments influenced by the Red River and Taiwan (Zhang et al., 2023), suggesting that gravity-driven processes are the main mechanism for transporting Pearl River-derived sediments into the trough. Sediments on the lower continental slope (SL-2) exhibit mixing with those from central Vietnam, consistent with the clay minerals studies (Liu et al., 2014a).

In the Northwest Sub-basin (AB-1), sediments show a pattern similar to those in the trough (SL-2), predominantly sourced from the Pearl River (approximately 80%, Figure 9). This suggests an eastward transportation trend via the gravity-driven Xisha Trough channel (Su et al., 2014; Zhao et al., 2015b; Lei et al., 2020). The topographic and sedimentation pattern of Xisha trough is similar to Valencia Trough, which receiving sediments from lateral on Ebro margin canyons, the eastward tilting of the Xisha Trough facilitates the longitudinal transport of the Red River sediments and northwestern SCS shelf sediments (mostly from the Pearl River) into the abyssal basin (Qin et al., 2015; Su et al., 2015). Unlike the Ebro margin, the closure of the SCS generates a well-developed deep-water current (Chen et al., 2016), transporting distal and fine-grained sediments (Liu et al., 2014a, 2016). Another different sediment transport scenario is also possible: the Pearl River Canyon system exports small amounts of sediments to the abyssal basin (Ding et al., 2013), with small canyons on the Yitong slope also potentially transporting Pearl River sediments (Figure 10). Sediments from Taiwan reach this location via deep-water currents (Liu et al., 2014a). However, current provenance datasets do not include samples from the Pearl River Canyon system and Yitong slope, limiting the identification of these scenarios.

Interestingly, Red River sediment abundance increases with water depth, consistent with observations in the water column (Liu et al., 2014a), whereas the trough and abyssal basin remain consistently without Red River-derived sediments (Figure 10). Given that Pearl River-derived sediments are present at all depths, the varying Red River sediment abundance is attributed to the changes in Pearl River contribution, suggesting Red River sediments are primarily transported by the intermediate water mass and the eastward deep-water current along the south wall of the Xisha Trough (Chen et al., 2016).

Typically, passive margin slopes connecting to open basins (e.g., the northern SCS margin, Mississippi margin, and Amazon margin) feature broad shelves and expansive abyssal plains (Taylor and Hayes, 1980; Nittrouer et al., 1995; Bentley et al., 2016; Liu et al., 2016).

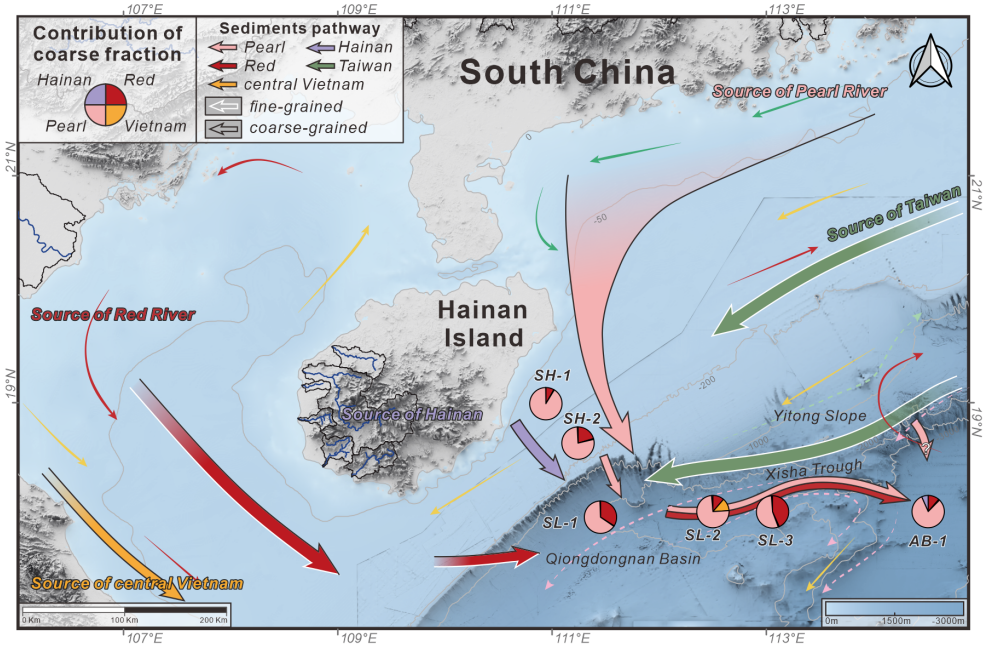

FIGURE 10
Transport pathways and source-to-sink process of sediments in the northwestern South China Sea. The pie plot shows the contribution of four sources calculated by the Monte Carlo model based on zircon geochronology. The pink arrow indicates the source of the Pearl River. The red arrow indicates the source of the Red River. The yellow arrow indicates the source of central Vietnam. The purple arrow indicates the source of Hainan. The green arrow indicates the source of Taiwan. The black outline of the arrows represents the coarse-grained fraction and the white outline corresponds to the fine-grained fraction.

However, in this study area, the continental slope connects to a relict rift-arm forming a tilting trough topography (Sun et al., 2009; Lei and Ren, 2016), inducing topography-controlled longitudinal sediment transportation, which is typically formed in active or immature passive margins (Shanmugam and Moiola, 1988). Surrounding rivers erode catchment rocks (e.g., the Pearl River contains mainly sedimentary rocks with small granites, and the Red River contains both granitic and sedimentary rocks), transporting sediment to the northern SCS. Zircons represent coarse-grained clastic sediments from Hainan Island and Pearl River settling on the broad shelf and then longitudinally transported into deep water (Figure 10). Fine-grained sediments, indicated by clay minerals from the distant Taiwan Island, are transported by surface and deep-water currents (Figure 10). This establishes a general source-to-sink sediment pattern on the northwestern continental margin of the SCS, influenced by coastal currents, deep-water currents, gravity-driven processes, and topographical constraints. This insight sheds light on the controlling processes of the source-to-sink system on the northwestern margin of the SCS.

7 Conclusion

The detrital zircon grains of the marine sediments from the northwestern SCS demonstrate that U-Pb geochronology is a reliable proxy for studying coarse-grained sediment provenance. The U-Pb age data from these sediments range from 3,062.9 to 41.5 Ma, with distinct age peaks at 140–154 Ma, 240–258 Ma, 425–452 Ma, and 738–991 Ma. A comparison of age spectra indicates sediment contributions from two major sources, the Pearl River and Red River, and two minor sources, the rivers of Hainan and central Vietnam.

Quantitative analysis reveals that sediments on the continental slope primarily originate from the Pearl River (55-75%), with lesser contributions from the Red River. Similarly, sediments in the abyssal basin also predominantly derive from the Pearl River. By integrating zircon geochronology and clay mineral analysis, it is evident that the coarse-grained fraction is more likely to be transported in deeper regions, whereas fine-grained sediments are carried by surface currents.

The study suggests that the Pearl River detritus is transported westward by coastal currents parallel to the shoreline, then descends through slope canyons, and is longitudinally transported along the Xisha Trough, likely driven by gravity flows, eventually depositing in the abyssal basin. By contrast, sediments from Hainan Island remain confined to the shallow shelf region due to limited southwestward transport and weak sediment supply. Red River sediments can reach the central Xisha Trough, predominantly transported by ocean currents.

The abyssal basin sediments may originate from multiple sources, including Pearl River-derived sediments transported along the Xisha Trough or through the Pearl River mouth canyon and Yitong slope canyons, as well as Taiwanese sediments transported by deep-water currents. This study underscores the importance of considering multiple sediment transport processes to understand sediment provenance and the source-to-sink process in the northern continental margin of the SCS, providing valuable insights for future research.

Data availability statement

The datasets presented in this study can be found in online repositories. The names of the repository/repositories and accession number(s) can be found in the article/Supplementary Material.

Author contributions

HC: Formal analysis, Investigation, Writing – original draft. CW: Conceptualization, Methodology, Project administration, Writing – review & editing. MS: Methodology, Writing – review & editing. YL: Resources, Writing – review & editing. LZ: Investigation, Writing – review & editing. JJ: Investigation, Writing – review & editing.

Funding

The author(s) declare financial support was received for the research, authorship, and/or publication of this article. This study was supported by funding from the National Natural Science Foundation of China (No. 42172111), the Projects of Southern Marine Science and Engineering Guangdong Laboratory (Zhuhai) (No. 311022005), and the “Fourteenth Five-Year Plan” Prospective Basic Major Scientific and Technological Projects of CNPC (No. 2021DJ4901).

Conflict of interest

The authors declare that the research was conducted in the absence of any commercial or financial relationships that could be construed as a potential conflict of interest.

Publisher’s note

Supplementary material

The Supplementary Material for this article can be found online at: https://www.frontiersin.org/articles/10.3389/fmars.2024.1427579/full#supplementary-material

References

Allen, P. A., Michael, N. A., D'arcy, M., Roda-Boluda, D. C., Whittaker, A. C., Duller, R. A., et al. (2015). Fractionation of grain size in terrestrial sediment routing systems. *Basin. Res.* 29, 180–202. doi: 10.1111/bre.12172

Alonso, B., Canals, M., Palanques, A., and Rehault, J.-P. (1995). A Deep-sea Channel in the Northwestern Mediterranean Sea: Morphology and seismic structure of the Valencia Channel and its surroundings. *Mar. Geophys. Res.* 17, 469–484. doi: 10.1007/bf01371788

Andersen, T. (2002). Correction of common lead in U–Pb analyses that do not report ^{204}Pb. *Chem. Geol.* 192, 59–79. doi: 10.1016/S0009-2541(02)00195-X

Bentley, S. J., Blum, M. D., Maloney, J., Pond, L., and Paulsell, R. (2016). The Mississippi River source-to-sink system: Perspectives on tectonic, climatic, and anthropogenic influences, Miocene to Anthropocene. *Earth-Sci. Rev.* 153, 139–174. doi: 10.1016/j.earscirev.2015.11.001

Blum, M., Rogers, K., Gleason, J., Najman, Y., Cruz, J., and Fox, L. (2018). Allogenic and autogenic signals in the stratigraphic record of the Deep-Sea bengal fan. *Sci. Rep.* 8, 7973. doi: 10.1016/s0016-7037(00)00352-5

Bodet, F., and Schärer, U. (2020). Evolution of the SE-Asian continent from U-Pb and Hf isotopes in single grains of zircon and baddeleyite from large river. *Geochim. Cosmochim. Acta.* 64, 2067–2091. doi: 10.1016/s0016-7037(00)00352-5

Cai, G., Li, S., Zhao, L., Zhong, L., and Chen, H. (2020). Clay minerals, Sr-Nd isotopes and provenance of sediments in the northwestern South China Sea. *J. Asian Earth Sci.* 202, 104531. doi: 10.1016/j.jseaes.2020.104531

Cao, L., Shao, L., Qiao, P., Zhao, Z., and Van Hinsbergen, D. J. J. (2018). Early Miocene birth of modern Pearl River recorded low-relief, high-elevation surface formation of SE Tibetan Plateau. *Earth Planet. Sci. Lett.* 496, 120–131. doi: 10.1016/j.epsl.2018.05.039

Cao, L., Shao, L., Van Hinsbergen, D. J. J., Jiang, T., Xu, D., and Cui, Y. (2023). Provenance and evolution of East Asian large rivers recorded in the East and South China Seas: A review. *Geol. Soc Am. Bull.* 135, 2723–2752. doi: 10.1130/b36559.1

Caracciolo, L. (2020). Sediment generation and sediment routing systems from a quantitative provenance analysis perspective: Review, application and future development. *Earth-Sci. Rev.* 209, 103226. doi: 10.1016/j.earscirev.2020.103226

Carter, A., Roques, D., Bristow, C., and Kinny, P. (2001). Understanding Mesozoic accretion in Southeast Asia: Significance of Triassic thermotectonism (Indosinian orogeny) in Vietnam. *Geology* 29, 211–214. doi: 10.1130/0091-7613(2001)029<0211:Umaisa>2.0.Co;2

Chen, H., Stow, D., Xie, X., Ren, J., Mao, K., Gao, Y., et al. (2021). Depositional architecture and evolution of basin-floor fan systems since the Late Miocene in the Northwest Sub-Basin, South China Sea. *Mar. Pet. Geol.* 126, 104803. doi: 10.1016/j.marpetgeo.2020.104803

Chen, H., Xie, X., Zhang, W., Shu, Y., Wang, D., Vandorpe, T., et al. (2016). Deep-water sedimentary systems and their relationship with bottom currents at the intersection of Xisha Trough and Northwest Sub-Basin, South China Sea. *Mar. Geol.* 378, 101–113. doi: 10.1016/j.margeo.2015.11.002

Clift, P. D., Carter, A., Campbell, I. H., Pringle, M. S., Van Lap, N., Allen, C. M., et al. (2006). Thermochronology of mineral grains in the Red and Mekong Rivers, Vietnam: Provenance and exhumation implications for Southeast Asia. *Geochem. Geophys. Geosyst.* 7, 2006GC001336. doi: 10.1029/2006gc001336

Clift, P. D., Giosan, L., Henstock, T. J., and Tabrez, A. R. (2014). Sediment storage and reworking on the shelf and in the Canyon of the Indus River-Fan System since the last glacial maximum. *Basin. Res.* 26, 183–202. doi: 10.1111/bre.12041

Clift, P. D., Long, H. V., Hinton, R., Ellam, R. M., Hannigan, R., Tan, M. T., et al. (2008). Evolving east Asian river systems reconstructed by trace element and Pb and Nd isotope variations in modern and ancient Red River-Song Hong sediments. *Geochem. Geophys. Geosyst.* 9, 2007GC001867. doi: 10.1029/2007gc001867

Ding, W., Li, J., Li, J., Fang, Y., and Tang, Y. (2013). Morphotectonics and evolutionary controls on the Pearl River Canyon system, South China Sea. *Mar. Geophys. Res.* 34, 221–238. doi: 10.1007/s11001-013-9173-9

Dodson, M. H., Compston, W., Williams, I. S., and Wilson, J. F. (2022). A search for ancient detrital zircons in Zimbabwean sediments. *J. Geol. Soc* 145, 977–983. doi: 10.1144/gsjgs.145.6.0977

Fyhn, M. B. W., Thomsen, T. B., Keulen, N., Knudsen, C., Rizzi, M., Bojesen-Koefoed, J., et al. (2019). Detrital zircon ages and heavy mineral composition along the Gulf of Tonkin - Implication for sand provenance in the Yinggehai-Song Hong and Qiongdongnan basins. *Mar. Pet. Geol.* 101, 162–179. doi: 10.1016/j.marpetgeo.2018.11.051

Gao, S., and Collins, M. B. (2014). Holocene sedimentary systems on continental shelves. *Mar. Geol.* 352, 268–294. doi: 10.1016/j.margeo.2014.03.021

Garzanti, E., Andò, S., and Vezzoli, G. (2009). Grain-size dependence of sediment composition and environmental bias in provenance studies. *Earth Planet. Sci. Lett.* 277, 422–432. doi: 10.1016/j.epsl.2008.11.007

Garzanti, E., Bayon, G., Dinis, P., Vermeesch, P., Pastore, G., Resentini, A., et al. (2022). The segmented zambezi sedimentary system from source to sink: 2. Geochemistry, clay minerals, and detrital geochronology. *J. Geol.* 130, 171–208. doi: 10.1086/719166

Gehrels, G. (2011). "Detrital zircon U-pb geochronology: current methods and new opportunities," in *Tectonics of Sedimentary Basins*. Eds. C. Busby and A. Azor (: Blackwell Publishing Ltd, New Jersey, United States), 45–62. doi: 10.1002/9781444347166.ch2

Gehrels, G. E., Valencia, V. A., and Ruiz, J. (2008). Enhanced precision, accuracy, efficiency, and spatial resolution of U-Pb ages by laser ablation-multicollector-inductively coupled plasma-mass spectrometry. *Geochem. Geophys. Geosyst.* 9, 1–13. doi: 10.1029/2007GC001805

Gilley, L. D., Harrison, T. M., Leloup, P. H., Ryerson, F. J., Lovera, O. M., and Wang, J. (2003). Direct dating of left-lateral deformation along the Red River shear zone, China and Vietnam. *J. Geophys. Res.-Solid. Earth* 108, 2001JB001726. doi: 10.1029/2001jb001726

Gong, Y., Pease, V., Wang, H., Gan, H., Liu, E., Ma, Q., et al. (2021). Insights into evolution of a rift basin: Provenance of the middle Eocene-lower Oligocene strata of the Beibuwan Basin, South China Sea from detrital zircon. *Sediment. Geol.* 419, 105908. doi: 10.1016/j.sedgeo.2021.105908

He, J., Garzanti, E., Cao, L., and Wang, H. (2020). The zircon story of the Pearl River (China) from Cretaceous to present. *Earth-Sci. Rev.* 201, 103078. doi: 10.1016/j.earscirev.2019.103078

Hoskin, P. W. O. (2003). The composition of zircon and igneous and metamorphic petrogenesis. *Rev. Mineral. Geochem.* 53, 27–62. doi: 10.2113/0530027

Hu, B., Li, J., Cui, R., Wei, H., Zhao, J., Li, G., et al. (2014). Clay mineralogy of the riverine sediments of Hainan Island, South China Sea: Implications for weathering and provenance. *J. Asian Earth Sci.* 96, 84–92. doi: 10.1016/j.jseaes.2014.08.036

Hu, D., Böning, P., Köhler, C. M., Hillier, S., Pressling, N., Wan, S., et al. (2012). Deep sea records of the continental weathering and erosion response to East Asian monsoon intensification since 14ka in the South China Sea. *Chem. Geol.* 326-327, 1–18. doi: 10.1016/j.chemgeo.2012.07.024

Hu, D., Clift, P. D., Boning, P., Hannigan, R., Hillier, S., Blusztajn, J., et al. (2013). Holocene evolution in weathering and erosion patterns in the Pearl River delta. *Geochem. Geophys. Geosyst.* 14, 2349–2368. doi: 10.1002/ggge.20166

Huang, D., Du, J., Deng, B., and Zhang, J. (2013). Distribution patterns of particle-reactive radionuclides in sediments off eastern hainan island, china: Implications for source and transport pathways. *Cont. Shelf Res.* 57, 10–17. doi: 10.1016/j.csr.2012.04.019

Huang, C., Wang, H., Yang, J., Ramezani, J., Yang, C., Zhang, S., et al. (2019). SA01 – A proposed zircon reference material for microbeam U-pb age and hf-O isotopic determination. *Geostand. Geoanal. Res.* 44, 103–123. doi: 10.1111/ggr.12307

Jia, J., Wang, C., Su, M., Yan, W., Zeng, L., and Cui, H. (2023). Provenance and dispersal patterns of sediments on the continental shelf of northern South China Sea: Evidence from detrital zircon geochronology. *Mar. Geol.* 457, 107013. doi: 10.1016/j.margeo.2023.107013

John, B. M., Zhou, X., and Li, J. (1990). Formation and tectonic evolution of Southeastern China and Taiwan: Isotopic and geochemical constraints. *Tectonophysics* 183, 145–160. doi: 10.1016/0040-1951(90)90413-3

Komar, P. D. (2007). "Chapter 1 the entrainment, transport and sorting of heavy minerals by waves and currents," in *Heavy Minerals in Use*. Eds. M. A. Mange and D. T. Wright (Elsevier, Amsterdam, Netherlands), 3–48. doi: 10.1016/S0070-4571(07)58001-5

Lei, C., Alves, T. M., Ren, J., and Tong, C. (2020). Rift structure and sediment infill of hyperextended continental crust: insights from 3D seismic and well data (Xisha trough, South China sea). *J. Geophys. Res.-Solid. Earth* 125, 2019JB018610. doi: 10.1029/2019jb018610

Lei, C., and Ren, J. (2016). Hyper-extended rift systems in the Xisha Trough, northwestern South China Sea: Implications for extreme crustal thinning ahead of a propagating ocean. *Mar. Pet. Geol.* 77, 846–864. doi: 10.1016/j.marpetgeo.2016.07.022

Lepvrier, C., Maluski, H., Van Tich, V., Leyreloup, A., Truong Thi, P., and Van Vuong, N. (2004). The Early Triassic Indosinian orogeny in Vietnam (Truong Son Belt and Kontum Massif); implications for the geodynamic evolution of IndoChina. *Tectonophysics* 393, 87–118. doi: 10.1016/j.tecto.2004.07.030

Lepvrier, C., Maluski, H., Van Vuong, N., Roques, D., Axente, V., and Rangin, C. (1997). Indosinian NW-trending shear zones within the Truong Son belt (Vietnam) ^{40}Ar-^{39}Ar Triassic ages and Cretaceous to Cenozoic overprints. *Tectonophysics* 283, 105–127. doi: 10.1016/s0040-1951(97)00151-0

Li, X., Li, Z., Li, W., and Wang, Y. (2006). Initiation of the Indosinian Orogeny in South China: Evidence for a Permian magmatic arc on Hainan Island. *J. Geol.* 114, 341–353. doi: 10.1086/501222

Li, G., Li, P., Liu, Y., Qiao, L., Ma, Y., Xu, J., et al. (2014). Sedimentary system response to the global sea level change in the East China Seas since the last glacial maximum. *Earth-Sci. Rev.* 139, 390–405. doi: 10.1016/j.earscirev.2014.09.007

Li, C., Lv, C., Chen, G., Zhang, G., Ma, M., Shen, H., et al. (2017). Source and sink characteristics of the continental slope-parallel Central Canyon in the Qiongdongnan

Basin on the northern margin of the South China Sea. *J. Asian Earth Sci.* 134, 1–12. doi: 10.1016/j.jseaes.2016.10.014

Li, M., Ouyang, T., Roberts, A. P., Heslop, D., Zhu, Z., Zhao, X., et al. (2018). Influence of sea level change and centennial east asian monsoon variations on Northern South China sea sediments over the past 36 kyr. *Geochem. Geophys. Geosyst.* 19, 1674–1689. doi: 10.1029/2017gc007321

Liu, C., Clift, P. D., Carter, A., Boning, P., Hu, Z., Sun, Z., et al. (2017). Controls on modern erosion and the development of the Pearl River drainage fa in the late Paleogene. *Mar. Geol.* 394, 52–68. doi: 10.1016/j.margeo.2017.07.011

Liu, J., Clift, P. D., Yan, W., Chen, Z., Chen, H., Xiang, R., et al. (2014a). Modern transport and deposition of settling particles in the northern South China Sea: Sediment trap evidence adjacent to Xisha Trough. *Deep. Sea. Res. Part I.* 93, 145–155. doi: 10.1016/j.dsr.2014.08.005

Liu, Y., Gao, S., Wang, Y., Yang, Y., Long, J., Zhang, Y., et al. (2014b). Distal mud deposits associated with the Pearl River over the northwestern continental shelf of the South China Sea. *Mar. Geol.* 347, 43–57. doi: 10.1016/j.margeo.2013.10.012

Liu, J., Tran, M. D., Tang, Y., Nguyen, Q. L., Tran, T. H., Wu, W., et al. (2012). Permo-Triassic granitoids in the northern part of the Truong Son belt, NW Vietnam: Geochronology, geochemistry and tectonic implications. *Gondwana. Res.* 22, 628–644. doi: 10.1016/j.gr.2011.10.011

Liu, X., Wei, G., Zou, J., Guo, Y., Ma, J., Chen, X. F., et al. (2018). Elemental and sr-nd isotope geochemistry of sinking particles in the northern south China sea: implications for provenance and transportation. *J. Geophys. Res.-Oceans.* 123, 9137–9155. doi: 10.1029/2018jc014312

Liu, Z., Yang, H., and Liu, Q. (2001). Regional dynamics of seasonal variability in the South China Sea. *J. Phys. Oceanogr.* 31, 272–284. doi: 10.1175/1520-0485(2001)031<0272:Rdosvi>2.0.Co;2

Liu, Z., Zhao, Y., Colin, C., Stattegger, K., Wiesner, M. G., Huh, C. A., et al. (2016). Source-to-sink transport processes of fluvial sediments in the South China Sea. *Earth-Sci. Rev.* 153, 238–273. doi: 10.1016/j.earscirev.2015.08.005

Lupker, M., France-Lanord, C., Galy, V., Lavé, J., and Kudrass, H. (2013). Increasing chemical weathering in the Himalayan system since the Last Glacial Maximum. *Earth Planet. Sci. Lett.* 365, 243–252. doi: 10.1016/j.epsl.2013.01.038

Milliman, J. D., and Farnsworth, K. L. (2013). *River discharge to the coastal ocean: a global synthesis* (New York: Cambridge University Press), 384.

Nittrouer, C. A., Kuehl, S. A., Sternberg, R. W., Figueiredo, A. G., and Faria, L. E. C. (1995). An introduction to the geological significance of sediment transport and accumulation on the Amazon continental shelf. *Mar. Geol.* 125, 177–192. doi: 10.1016/0025-3227(95)00075-a

Qin, Z., Wu, S., Wang, D., Li, W., Gong, S., Mi, L., et al. (2015). Mass transport deposits and processes in the north slope of the Xisha Trough, northern South China Sea. *Acta Oceanolog. Sin.* 34, 117–125. doi: 10.1007/s13131-015-0608-9

Qu, T. (2000). Upper-layer circulation in the south China sea. *J. Phys. Oceanogr.* 30, 1450–1460. doi: 10.1175/1520-0485(2000)030<1450:Ulcits>2.0.Co;2

Qu, T., Girton, J. B., and Whitehead, J. A. (2006). Deepwater overflow through Luzon Strait. *J. Geophys. Res.* 111, 2005JC003139. doi: 10.1029/2005jc003139

Roger, F. O., Leloup, P. H., Jolivet, M., Lacassin, R., Trinh, P. T., Brunel, M., et al. (2000). Long and complex thermal history of the Song Chay metamorphic dome (Northern Vietnam) by multi-system geochronology. *Tectonophysics* 321, 449–466. doi: 10.1016/S0040-1951(00)00085-8

Roger, F., Maluski, H. R., Leyreloup, A., Lepvrier, C., and Truong Thi, P. (2007). U–Pb dating of high temperature metamorphic episodes in the Kon Tum Massif (Vietnam). *J. Asian Earth Sci.* 30, 565–572. doi: 10.1016/j.jseaes.2007.01.005

Romans, B. W., Castelltort, S., Covault, J. A., Fildani, A., and Walsh, J. P. (2016). Environmental signal propagation in sedimentary systems across timescales. *Earth-Sci. Rev.* 153, 7–29. doi: 10.1016/j.earscirev.2015.07.012

Saylor, J. E., Jordan, J. C., Sundell, K. E., Wang, X., Wang, S., and Deng, T. (2017). Topographic growth of the Jishi Shan and its impact on basin and hydrology evolution, NE Tibetan Plateau. *Basin. Res.* 30, 544–563. doi: 10.1111/bre.12264

Saylor, J. E., and Sundell, K. E. (2016). Quantifying comparison of large detrital geochronology data sets. *Geosphere* 12, 203–220. doi: 10.1130/ges01237.1

Schärer, U., Zhang, L., and Tapponnier, P. (1994). Duration of strike-slip movements in large shear zones: The Red River belt, China. *Earth Planet. Sci. Lett.* 126, 379–397. doi: 10.1016/0012-821x(94)90119-8

Sewell, R. J., and Campbell, S. D. G. (2022). Geochemistry of coeval Mesozoic plutonic and volcanic suites in Hong Kong. *J. Geol. Soc* 154, 1053–1066. doi: 10.1144/gsjgs.154.6.1053

Shanmugam, G., and Moiola, R. J. (1988). Submarine fans: Characteristics, models, classification, and reservoir potential. *Earth-Sci. Rev.* 24, 383–428. doi: 10.1016/0012-8252(88)90064-5

Sharman, G. R., Graham, S. A., Grove, M., Kimbrough, D. L., and Wright, J. E. (2015). Detrital zircon provenance of the Late Cretaceous–Eocene California forearc: Influence of Laramide low-angle subduction on sediment dispersal and paleogeography. *Geol. Soc Am. Bull.* 127, 38–60. doi: 10.1130/b31065.1

Sharman, G. R., and Johnstone, S. A. (2017). Sediment unmixing using detrital geochronology. *Earth Planet. Sci. Lett.* 477, 183–194. doi: 10.1016/j.epsl.2017.07.044

Shi, M., Lin, F., Fan, W., Deng, Q., Cong, F., Tran, M., et al. (2015). Zircon U–Pb ages and geochemistry of granitoids in the Truong Son terrane, Vietnam: Tectonic and metallogenic implications. *J. Asian Earth Sci.* 101, 101–120. doi: 10.1016/j.jseaes.2015.02.001

Sláma, J., Košler, J., Condon, D. J., Crowley, J. L., Gerdes, A., Hanchar, J. M., et al. (2008). Plešovice zircon — A new natural reference material for U–Pb and Hf isotopic microanalysis. *Chem. Geol.* 249, 1–35. doi: 10.1016/j.chemgeo.2007.11.005

Su, J. (2004). Overview of the South China Sea circulation and its influence on the coastal physical oceanography outside the Pearl River Estuary. *Cont. Shelf. Res.* 24, 1745–1760. doi: 10.1016/j.csr.2004.06.005

Su, M., Hsiung, K.-H., Zhang, C., Xie, X., Yu, H.-S., and Wang, Z. (2015). The linkage between longitudinal sediment routing systems and basin types in the northern South China Sea in perspective of source-to-sink. *J. Asian Earth Sci.* 111, 1–13. doi: 10.1016/j.jseaes.2015.05.011

Su, M., Xie, X., Xie, Y., Wang, Z., Zhang, C., Jiang, T., et al. (2014). The segmentations and the significances of the Central Canyon System in the Qiongdongnan Basin, northern South China Sea. *J. Asian Earth Sci.* 79, 552–563. doi: 10.1016/j.jseaes.2012.12.038

Sun, Z., Zhong, Z., Keep, M., Zhou, D., Cai, D., Li, X., et al. (2009). 3D analogue modeling of the South China Sea: A discussion on breakup pattern. *J. Asian Earth Sci.* 34, 544–556. doi: 10.1016/j.jseaes.2008.09.002

Sun, Z., Zhou, D., Zhong, Z., Xia, B., Qiu, X., Zeng, Z., et al. (2006). Research on the dynamics of the South China Sea opening: Evidence from analogue modeling. *Sci. China-Earth. Sci.* 49, 1053–1069. doi: 10.1007/s11430-006-1053-6

Sundell, K. E., and Saylor, J. E. (2017). Unmixing detrital geochronology age distributions. *Geochem. Geophys. Geosyst.* 18, 2872–2886. doi: 10.1002/2016gc006774

Taylor, B., and Hayes, D. E. (1980). "The tectonic evolution of the South China Basin," in *The tectonic and Geologic Evolution of Southeast Asian Seas and Islands*. Ed. D. E. Hayes (American Geophysical Union, Washington, D.C., United States), 89–104. doi: 10.1029/GM023p0089

Taylor, B., and Hayes, D. E. (1983). Origin and history of the south China sea basin. *Washington. DC. Am. Geophys. Union. Geophys. Monograph. Ser.* 27, 23–56. doi: 10.1029/GM027p0023

Van Hoang, L., Wu, F., Clift, P. D., Wysocka, A., and Swierczewska, A. (2009). Evaluating the evolution of the Red River system based on in *situ* U-Pb dating and Hf isotope analysis of zircons. *Geochem. Geophys. Geosyst.* 10, 2009GC002819. doi: 10.1029/2009gc002819

Vermeesch, P. (2012). On the visualisation of detrital age distributions. *Chem. Geol.* 312–313, 190–194. doi: 10.1016/j.chemgeo.2012.04.021

Vermeesch, P. (2013). Multi-sample comparison of detrital age distributions. *Chem. Geol.* 341, 140–146. doi: 10.1016/j.chemgeo.2013.01.010

Vermeesch, P. (2018). IsoplotR: A free and open toolbox for geochronology. *Geosci. Front.* 9, 1479–1493. doi: 10.1016/j.gsf.2018.04.001

Wang, Y., Fan, W., Zhang, G., and Zhang, Y. (2013b). Phanerozoic tectonics of the South China Block: Key observations and controversies. *Gondwana. Res.* 23, 1273–1305. doi: 10.1016/j.gr.2012.02.019

Wang, Y., Fan, W., Zhao, G., Ji, S., and Peng, T. (2007b). Zircon U–Pb geochronology of gneissic rocks in the Yunkai massif and its implications on the Caledonian event in the South China Block. *Gondwana. Res.* 12, 404–416. doi: 10.1016/j.gr.2006.10.003

Wang, Q., Li, X., Jia, X., Wyman, D., Tang, G., Li, Z., et al. (2012). Late Early Cretaceous adakitic granitoids and associated magnesian and potassium-rich mafic enclaves and dikes in the Tunchang–Fengmu area, Hainan Province (South China): Partial melting of lower crust and mantle, and magma hybridization. *Chem. Geol.* 328, 222–243. doi: 10.1016/j.chemgeo.2012.04.029

Wang, C., Liang, X., Foster, D. A., Tong, C., Liu, P., Liang, X., et al. (2019). Linking source and sink: Detrital zircon provenance record of drainage systems in Vietnam and the Yinggehai-Song Hong Basin, South China Sea. *Geol. Soc Am. Bull.* 131, 191–204. doi: 10.1130/B32007.1

Wang, C., Liang, X., Xie, Y., Tong, C., Pei, J., Zhou, Y., et al. (2014). Provenance of Upper Miocene to Quaternary sediments in the Yinggehai-Song Hong Basin, South China Sea: Evidence from detrital zircon U–Pb ages. *Mar. Geol.* 355, 202–217. doi: 10.1016/j.margeo.2014.06.004

Wang, C., Liang, X., Zhou, Y., Fu, J., Jiang, Y., Dong, C., et al. (2015). Construction of age frequencies of provenances on the eastern side of the Yinggehai Basin: Studies of LA-ICP-MS U-Pb ages of detrital zircons from six modern rivers, western Hainan, China. *Earth Sci. Front.* 22, 277–289. doi: 10.13745/j.esf.2015.04.028

Wang, D., Wang, Q., Zhou, W., Cai, S., Li, L., and Hong, B. (2013a). An analysis of the current deflection around Dongsha Islands in the northern South China Sea. *J. Geophys. Res.-Oceans.* 118, 490–501. doi: 10.1029/2012jc008429

Wang, D., Xiao, J., Shu, Y., Xie, Q., Chen, J., and Wang, Q. (2016). Progress on deep circulation and meridional overturning circulation in the South China Sea. *Sci. China-Earth. Sci.* 59, 1827–1833. doi: 10.1007/s11430-016-5324-6

Wang, G., Xie, S., Qu, T., and Huang, R. (2011). Deep south China sea circulation. *Geophys. Res. Lett.* 38, 2010GL046626. doi: 10.1029/2010gl046626

Wang, X., Zhou, J., Griffin, W. L., Wang, R., Qiu, H., O'reilly, S. Y., et al. (2007a). Detrital zircon geochronology of Precambrian basement sequences in the Jiangnan orogen: Dating the assembly of the Yangtze and Cathaysia Blocks. *Precambrian. Res.* 159, 117–131. doi: 10.1016/j.precamres.2007.06.005

Xia, H., Liu, Y., and Yang, Y. (2009). Internal-wave characteristics of strong bottom currents at the sand-wave zone of the northern South China Sea and its role in sand-wave motion. *J. Trop. Oceanogr.* 28, 15–22. doi: 10.11978/j.issn.1009-5470.2009.06.015

Xie, C., Zhu, J., Ding, S., Zhang, Y., Fu, T., and Li, Z. (2006). Identification of Hercynian shoshonitic intrusive rocks in central Hainan Island and its geotectonic implications. *Chin. Sci. Bull.* 51, 2507–2519. doi: 10.1007/s11434-006-2122-0

Xu, B., Jiang, S., Wang, R., Ma, L., Zhao, K., and Yan, X. (2015). Late Cretaceous granites from the giant Dulong Sn-polymetallic ore district in Yunnan Province, South China: Geochronology, geochemistry, mineral chemistry and Nd–Hf isotopic compositions. *Lithos* 218–219, 54–72. doi: 10.1016/j.lithos.2015.01.004

Xu, F., Hu, B., Dou, Y., Liu, X., Wan, S., Xu, Z., et al. (2017). Sediment provenance and paleoenvironmental changes in the northwestern shelf mud area of the South China Sea since the mid-Holocene. *Cont. Shelf Res.* 144, 21–30. doi: 10.1016/j.csr.2017.06.013

Xue, H., Chai, F., Pettigrew, N., Xu, D., Shi, M., and Xu, J. (2004). Kuroshio intrusion and the circulation in the South China Sea. *J. Geophys. Res.-Oceans.* 109, 2002JC001724. doi: 10.1029/2002jc001724

Yan, Q., Metcalfe, I., and Shi, X. (2017). U-Pb isotope geochronology and geochemistry of granites from Hainan Island (northern South China Sea margin): Constraints on late Paleozoic-Mesozoic tectonic evolution. *Gondwana. Res.* 49, 333–349. doi: 10.1016/j.gr.2017.06.007

Zhang, L., Ren, Z., Xia, X., Wang, C., and Qian, S. (2018). An improved U-Pb age dating method for detrital zircon by LA-MC-ICP-MS. *Geochem. J.* 52, 433–439. doi: 10.2343/geochemj.2.0529

Zhang, L., and Schärer, U. (1999). Age and origin of magmatism along the Cenozoic Red River shear belt, China. *Contrib. Mineral. Petrol.* 134, 67–85. doi: 10.1007/s004100050469

Zhang, Q., Swann, G. E. A., Liu, J., Gao, W., Cui, Z., Li, G., et al. (2023). Sea level controls on the provenance of fine-grained sediments in the Xisha Trough, northwestern South China Sea over the last ~30 ka. *Mar. Geol.* 466, 107184. doi: 10.1016/j.margeo.2023.107184

Zhang, J., Wang, D., Jennerjahn, T., and Dsikowitzky, L. (2013). Land–sea interactions at the east coast of Hainan Island, South China Sea: A synthesis. *Cont. Shelf. Res.* 57, 132–142. doi: 10.1016/j.csr.2013.01.004

Zhao, M., Shao, L., and Qiao, P. (2015a). Characteristics of detrital zircon U-Pb geochronology of the Pearl River Sands and its implication on provenances. *J. Tongji. Univ. Nat. Sci.* 43, 915–923. doi: 10.11908/j.issn.0253-374x.2015.06.018

Zhao, Z., Sun, Z., Wang, Z., Sun, Z., Liu, J., and Zhang, C. (2015b). The high resolution sedimentary filling in Qiongdongnan Basin, Northern South China Sea. *Mar. Geol.* 361, 11–24. doi: 10.1016/j.margeo.2015.01.002

Zhong, Y., Chen, Z., Li, L., Liu, J., Li, G., Zheng, X., et al. (2017b). Bottom water hydrodynamic provinces and transport patterns of the northern South China Sea: Evidence from grain size of the terrigenous sediments. *Cont. Shelf. Res.* 140, 11–26. doi: 10.1016/j.csr.2017.01.023

Zhong, L., Li, G., Yan, W., Xia, B., Feng, Y., Miao, L., et al. (2017a). Using zircon U–Pb ages to constrain the provenance and transport of heavy minerals within the northwestern shelf of the South China Sea. *J. Asian Earth Sci.* 134, 176–190. doi: 10.1016/j.jseaes.2016.11.019

Zhong, G., and Peng, X. (2021). Transport and accumulation of plastic litter in submarine canyons—The role of gravity flows. *Geology* 49, 581–586. doi: 10.1130/g48536.1

Zhou, X. M., and Li, W. X. (2000). Origin of late mesozoic igneous rocks in Southeastern China: Implications for lithosphere subduction and underplating of mafic magmas. *Tectonophysics* 326, 269–287. doi: 10.1016/S0040-1951(00)00120-7

Zhou, Y., Liang, X., Kröner, A., Cai, Y., Shao, T., Wen, S., et al. (2015). Late Cretaceous lithospheric extension in SE China: Constraints from volcanic rocks in Hainan Island. *Lithos* 232, 100–110. doi: 10.1016/j.lithos.2015.06.028

Zhu, M., Graham, S., Pang, X., and Mchargue, T. (2010). Characteristics of migrating submarine canyons from the middle Miocene to present: Implications for paleoceanographic circulation, northern South China Sea. *Mar. Pet. Geol.* 27, 307–319. doi: 10.1016/j.marpetgeo.2009.05.005

Zhu, Y., Sun, J., Wang, Y., Li, S., Xu, T., Wei, Z., et al. (2019). Overview of the multi-layer circulation in the South China Sea. *Prog. Oceanogr.* 175, 171–182. doi: 10.1016/j.pocean.2019.04.001